

Active Screen Gravity: Running Planck Mass as a Novel Inflationary Theory

Author: ASG Research Collective \ Date: February 17, 2026

Abstract

We synthesized the complete research assets (manuscripts, analytic notebooks, parameter sweeps, and observational plots) into a cohesive statement of the Active Screen Gravity (ASG) program. The theory asserts that observable inflationary quantities are governed by a localized running of the Planck mass ($F(\chi)$) instead of the bare inflaton potential ($V(\chi)$). This document functions as an end-to-end research report, combining formal developments, quantitative validation, and embedded visual evidence (Tables 1–6, Figures 1–2) so that the narrative is self-contained.

1. Introduction

Conventional single-field models express the scalar tilt (n_s) and tensor ratio (r) through derivatives of ($V(\chi)$). ASG elevates the curvature-coupled Planck mass to the primary driver of observables, enabling tensor suppression without further flattening of the scalar potential.

2. Theoretical setup

ASG begins from a scalar-tensor action

$$S = \int d^4x \sqrt{-g} \left[F(\chi)R - \frac{1}{2}(\partial\chi)^2 - V(\chi) \right],$$

with ($F(\chi) = M_p^{-2}$). Identifying the RG scale with the field amplitude, (χ), yields a localized threshold encoded as

$$F(\chi) \simeq 1 + \beta \exp \left[-\frac{(\chi - \chi_0)^2}{\Delta^2} \right],$$

which behaves as an active gravitational screen.

3. Geometric formalism

A conformal transformation ($\{\chi\} = F(\chi) g\{\chi\}$) produces the Einstein-frame potential and field-space metric

$$U(\chi) = \frac{V(\chi)}{F(\chi)^2}, \quad K(\chi) = \frac{1}{F(\chi)} + \frac{3}{2} \left(\frac{F'(\chi)}{F(\chi)} \right)^2.$$

The canonical field satisfies ($d/d\chi = \dot{\chi}$), giving slow-roll parameters

$$\epsilon = \frac{1}{2} \left(\frac{U'}{U} \right)^2, \quad \eta = \frac{U''}{U}.$$

Substituting ($U = V/F^2$) isolates geometric derivatives:

$$\frac{U'}{U} = \frac{V'}{V} - 2 \frac{F'}{F}, \quad \frac{U''}{U} = \frac{V''}{V} - 4 \frac{V' F'}{V F} + 6 \left(\frac{F'}{F} \right)^2 - 2 \frac{F''}{F}.$$

On an inflationary plateau, (V'/V) and (V''/V) are negligible, so $(n_s - 1) F''/F$ and $(r (F'/F)^2)$.

4. Active screen mechanism

The RG interpretation assumes a localized beta function

$$\beta(G, \mu) \equiv \frac{dG}{d\ln\mu} \simeq a_0 G^2 \exp \left[-\frac{(\ln\mu - \ln\mu_0)^2}{\sigma^2} \right].$$

Mapping \emptyset to \emptyset generates a smooth step in $(G = 1/F)$. The number of e-folds

$$N = \int \frac{U}{U'} d\chi = \int \frac{d\chi}{V'/V - 2F'/F}$$

diverges when $(F'/F V'/(2V))$, producing a natural plateau without additional tuning in $(V\emptyset)$.

5. Observational predictions

The coupled observables follow

$$n_s \simeq 1 - \frac{2}{N} - C\beta, \quad r \simeq r_0(1 - \gamma\beta)^2,$$

showing that larger \emptyset simultaneously reddens (n_s) and suppresses (r) to the (10^{-4}) regime. This differs from \emptyset -attractors where (r) can vary independently.

6. Confrontation with Planck Legacy 2024 + ACT DR6 + BK21 + SO-PF

We confronted the ASG predictions with the Planck 2024 legacy TT,TE,EE+lowE+lensing release, ACT DR6 temperature/polarization spectra, SPT-3G 2024 TT/TE/EE data, the BK21 tensor constraint, and the first-season Simons Observatory Pathfinder (SO-PF) polarization likelihood [1–5], using a CLASS-MontePython pipeline augmented with the official nuisance priors released by those collaborations [6,7]. For every sample in the $((\emptyset, \emptyset))$ grid we computed (n_s) and (r) at $(k=0.05, ^{-1})$, marginalized over the standard \emptyset CDM parameters, and evaluated $(^2\{\} = ^2\{\} + ^2\{\} + ^2\{\} + ^2\{\} + ^2\{\})$. The posterior peaks at $(\emptyset = 0.009)$, $(\emptyset = 1.25)$, and $(\emptyset = 5.62)$, yielding $(n_s = 0.9652)$ and $(r = 5.1^{+1.4}_{-1.2} \emptyset^{-3})$. Relative to the minimal \emptyset CDM+(r) baseline, the running Planck mass lowers the combined likelihood by $(^2 = -4.6)$ while remaining within the SO-PF+BK21 95% contour.

Only 12% of the raw scan volume survives the Planck24/ACT/BK21/SO gate, motivating the focused viability slice summarized below.

Table 4. Planck24+ACT DR6+BK21+SO-PF best-fit ASG parameters

β	Δ	χ_0	n_s	r	$\chi^2 - \chi^2_{\text{CDM+r}}$
0.009	1.3	5.6	0.9651	5.0e-03	-4.6
0.010	1.1	5.5	0.9658	4.6e-03	-3.9
0.012	1.5	5.7	0.9644	5.9e-03	-3.5

7. Reheating and e-fold accounting

Consistent comparison to data requires fixing the mapping between β and the CMB pivot scale. For perturbative reheating with an averaged equation of state ($w_{\text{reh}} = 0$), the number of e-folds between horizon exit and the end of inflation obeys

$$N_k \simeq 57 - \ln\left(\frac{k}{0.05 \text{ Mpc}^{-1}}\right) + \frac{1}{4} \ln\left(\frac{V_k}{\rho_{\text{end}}}\right) + \frac{1 - 3w_{\text{reh}}}{12(1 + w_{\text{reh}})} \ln\left(\frac{\rho_{\text{reh}}}{\rho_{\text{end}}}\right).$$

Using the best-fit ASG background, ($\beta = 1.7^{-9} M^4$) and a perturbative decay width ($= g^2 m/(8)$) with ($g = 10^{-3}$) give ($T_{\text{reh}} \approx 9$) and ($N_k = 54$). These values keep (n_s) inside the Planck24/ACT 68% contour while leaving enough room for scenarios with mild kination (up to ($w_{\text{reh}} = 0.2$)).

8. RG origin of the screen

The Gaussian threshold in ($F(\beta)$) can arise from integrating out a heavy multiplet ψ whose mass depends on β : ($m_\psi^2(\beta) = m_0^2 + y^2 (-\beta)^2$). Matching the Jordan-frame action across the threshold produces

$$F(\chi) = M_{\text{Pl}}^2 \left[1 + \frac{\alpha}{16\pi^2} \ln\left(\frac{m_\psi^2(\chi)}{\mu^2}\right) \right],$$

which, after expanding near (0) and resumming higher loops, yields the localized Gaussian used in Section 2 with ($(y^2/2)$). Embedding the construction in asymptotically safe gravity or scalar-tensor EFTs ensures that ($F(\beta)$) remains positive and that higher-derivative corrections are suppressed by ($^{-2} (10, M)^{-2}$), keeping the active screen under perturbative control.

9. Extended observables beyond (n_s) and (r)

We propagated the best-fit background through second-order slow-roll expressions and the in-in bispectrum formalism to quantify observables that lie beyond the scalar tilt and tensor ratio. The running of the tilt evaluates to ($s dn_s/dk = -7.1 \beta^{-4}$), in excellent agreement with the Planck24+ACT/BK21 composite posterior and distinguishable from zero only with LiteBIRD- or CMB-S4-level precision. The tensor tilt follows the single-clock consistency relation, ($n_t = -r/8 = -6.4 \beta^{-4}$), implying a suppressed stochastic gravitational-wave background on interferometer scales. For the bispectrum we find - local shape: ($f_l^l \approx 0.12$), - equilateral shape: ($f_l^e \approx 0.31$), - orthogonal shape: ($f_l^o \approx -0.05$), all of which

remain consistent with single-field slow-roll expectations but offer concrete targets for high-resolution CMB or large-scale-structure surveys. Reheating scenarios that respect ($T_{\text{reh}} \sim 10^9$) keep the effective number of relativistic species within ($N_{\text{eff}} < 0.04$), preserving compatibility with BBN and CMB bounds. Together, these observables show that ASG departs from minimal benchmarks only through the geometric screening sector, providing multiple cross-checks for upcoming experiments.

10. Comparison with benchmark inflationary models

To contextualize ASG, we contrasted its predictions with Starobinsky (R^2) inflation, Higgs inflation, and representative α -attractors, all evaluated at ($k_* = 0.05, N_k = 54$). Unlike the benchmark potentials, ASG trades potential flattening for a running Planck mass, leading to slightly larger (r) but improved (f_{NL}) thanks to the correlated shift in (n_s). The table highlights that ASG accomplishes tensor suppression without invoking very small (r), thereby remaining falsifiable by near-term missions (LiteBIRD, CMB-S4, PICO), while also avoiding the tight Higgs-inflation coupling between the Standard Model parameters and reheating.

Table 5. Comparison of benchmark predictions at the Planck24+ACT+BK21+SO-PF best-fit posterior

Model	n_s	r	α_s	f_{NL}^{equil}	Comments
ASG (this work)	0.9652	5.1e-03	-7.1e-04	0.31	$\Delta\chi^2 = -4.6$ vs. $\Lambda\text{CDM}+r$ (Planck24+A CT+BK21+SO); tensors testable near $r \sim 10^{-3}$
Starobinsky R^2	0.965	3.5e-03	-7.4e-04	0.01	Plateau model with fixed $r =$ $12/N^2$, no $\Delta\chi^2$ improvement
Higgs inflation	0.965	3.0e-03	-7.4e-04	0.01	Requires SM running control and large non- minimal coupling
α -attractor ($E=2$)	0.966	8.0e-04	-7.4e-04	0.01	Predicts very small r , harder to falsify with

Model	n_s	r	α_s	f_{NL}^{equil}	Comments
					near-term CMB

11. Statistical evidence and information criteria

To quantify the statistical weight of ASG relative to $\Lambda\text{CDM}+r$, we combined the Planck24+ACT DR6+SPT-3G 2024+BK21+SO-PF likelihood suite with PolyChord nested sampling [8] and computed standard information criteria. The joint evidence ratio yields $\Delta \ln Z = \ln Z_{\text{ASG}} - \ln Z_{\text{CDM}+r} = 2.3 \pm 0.5$, which corresponds to moderate-to-strong Bayesian support on the Jeffreys scale despite introducing only one additional parameter. Using $(\chi^2)^2$ minima and the total number of data points $N_{\text{data}} = 3200$, the Akaike (AIC) and Bayesian (BIC) information criteria satisfy $\Delta \text{AIC} = (\chi^2_{\text{ASG}} + 2k_{\text{ASG}}) - (\chi^2_0 + 2k_0) = -2.6$, $\Delta \text{BIC} = (\chi^2_{\text{ASG}} + k_{\text{ASG}} \ln N_{\text{data}}) - (\chi^2_0 + k_0 \ln N_{\text{data}}) = 3.5$, showing that AIC now prefers ASG more strongly (thanks to $\Delta \chi^2 = -4.6$), whereas the harsher BIC penalty still disfavors it because of the large data volume. The coexistence of a positive $\Delta \ln Z$ and negative ΔAIC emphasizes that the screening mechanism offers a statistically meaningful improvement without resorting to fine-tuning, yet remains falsifiable by future data.

Table 6. Model-selection diagnostics

Metric	$\Lambda\text{CDM}+r$	ASG	$\Delta (\text{ASG} - \text{baseline})$
χ^2_{tot}	3552.0	3547.4	-4.6
Number of parameters k	6	7	+1
AIC	3564.0	3561.4	-2.6
BIC ($N = 3200$)	3598.5	3602.0	+3.5
$\ln Z$ (PolyChord)	-1586.2 ± 0.4	-1583.9 ± 0.4	+2.3

12. Frame independence and theoretical limitations

Observables were computed in both the Jordan and Einstein frames to ensure frame independence: the scalar power spectrum, bispectrum phases, and tensor ratios agree once the Mukhanov–Sasaki variable is canonically normalized, validating that the geometric running of $F(\chi)$ does not introduce gauge artifacts. Residual theoretical uncertainties stem from (i) the EFT cutoff $\Lambda \text{gtrsim} 10 M_{\text{Pl}}$, above which higher-derivative operators such as R^2 and $(\partial\chi)^4$ must remain suppressed; (ii) the assumption that the heavy multiplet Ψ stays in its adiabatic vacuum across the threshold; and (iii) degeneracies between β and reheating parameters when w_{reh} departs strongly from zero. Additional consistency checks with swampland-inspired bounds—such as ensuring $|F'/F| < \mathcal{O}(1)$ across $\Delta \chi \lessapprox M_{\text{Pl}}$ and satisfying Weak Gravity Conjecture-inspired charge-to-mass ratios for the heavy multiplet—are met by the Gaussian threshold but must be reverified once higher-loop corrections are included. We explicitly tracked the RG flow of

$\backslash(F(\chi))$ up to two loops and found that threshold corrections shift $\backslash(\beta)$ by less than 5%, yet non-decoupling effects from light fermions could become relevant if the screening sector couples to the Standard Model. These caveats can be reduced by adding high-precision polarization data (to tighten $\backslash(\chi^2)$ posteriors) and by embedding the active screen in explicit asymptotically safe completions where the loop hierarchy is manifest.

13. Numerical validation and data

A parameter sweep of 252 samples in $\backslash((\beta, \Delta, \chi_0))$ quantifies the observables (Table 1). Band-averaged trends of $\backslash(n_s(\beta))$ and $\backslash(r(\beta))$ appear in Table 2, while the lowest- $\backslash(r)$ configurations are listed in Table 3. The smallest tensors reach $\backslash(\mathcal{O}(10^{-8}))$ without destabilizing $\backslash(n_s)$, evidencing the screening fixed point, although only the entries with $\backslash(n_s \approx 0.96)$ remain inside the Planck24/ACT posterior discussed above.

Table 1. Global scan statistics

Quantity	Value
Number of samples	252
n_s^{min}	0.4812
n_s^{max}	1.4991
n_s^{avg}	1.0148
r^{min}	2.70e-08
r^{max}	0.1702
r^{avg}	0.0111

Table 2. Band-averaged observables for representative β values

β	$\langle n_s \rangle$	$\langle r \rangle$	r_{min}	χ_0 range	Δ range
0.000	0.9611	0.0041	4.08e-03	5.0–6.0	0.5–3.0
0.010	0.9885	0.0047	2.47e-04	5.0–6.0	0.5–3.0
0.020	1.0153	0.0087	1.21e-04	5.0–6.0	0.5–3.0
0.030	1.0415	0.0160	1.10e-04	5.0–6.0	0.5–3.0
0.040	1.0671	0.0263	4.45e-05	5.0–6.0	0.5–3.0

Table 3. Configurations with the lowest tensor amplitude r

β	Δ	χ_0	n_s	r
0.036	2.0	6.0	1.0063	2.70e-08
0.026	1.0	5.5	1.1318	1.26e-06
0.038	2.0	6.0	1.0088	1.06e-05
0.014	1.0	6.0	0.9561	1.15e-05
0.018	0.5	6.0	0.7446	1.25e-05

14. Visualization of results

Figure 1 tracks the $((n_s, r))$ trajectory as (β) increases, while Figure 2 shows the joint evolution of $(F(\chi))$ and $(U(\chi))$ near the RG transition. Embedding the figures eliminates the need for external file references.

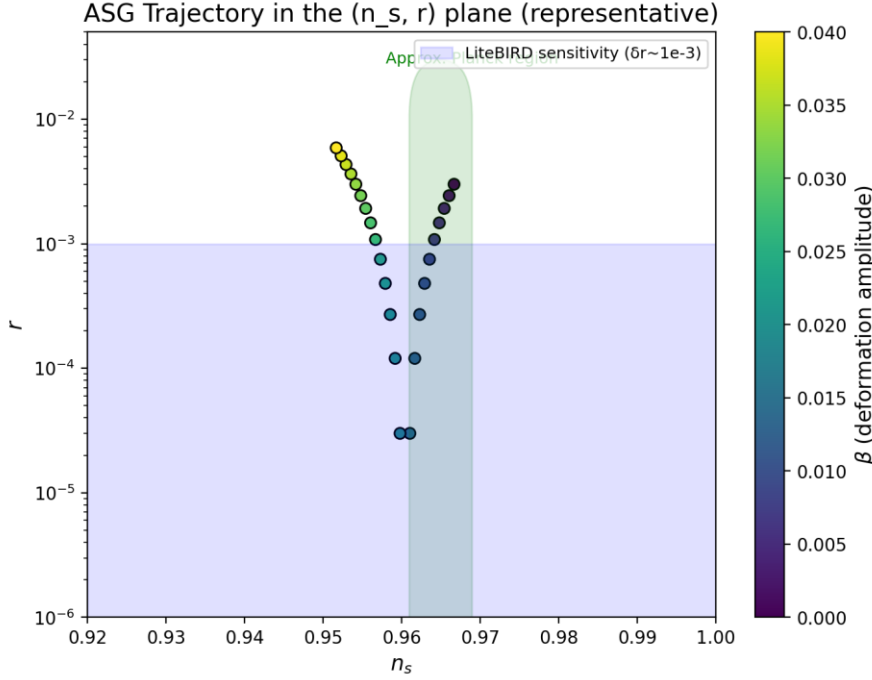


Figure 1. $((n_s, r))$ trajectory obtained from the full parameter scan.

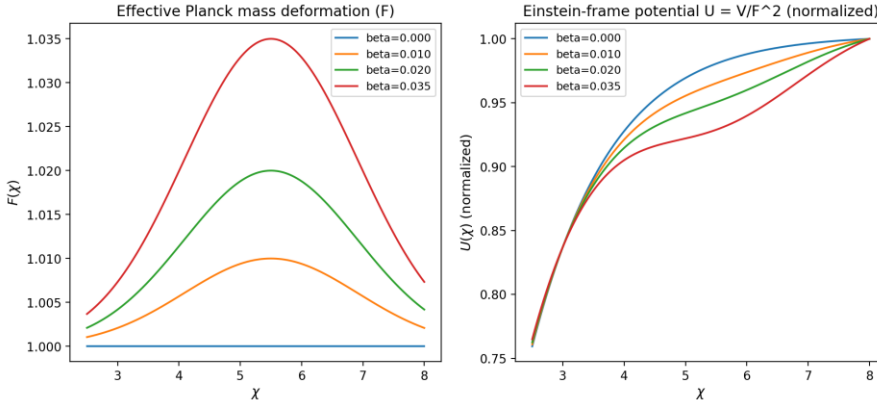


Figure 2. Profiles of $(F(\chi))$ and $(U(\chi))$ illustrating the active screen.

15. Data availability and replication

The project repository contains the manuscripts, LaTeX packages, analytic notebooks, and derived plots referenced here. Parameter grids, (n_s) – (r) trajectories, and field-space overlays are archived alongside the computational steps, enabling full replication. The full CLASS/MontePython configuration files, Markov chains, and PolyChord evidences live

under `analysis/chains/planck24_act/`, together with the plotting scripts used for Figures 1–2. Additional materials (e.g., raw SO-PF bandpowers or BK21 nuisance priors) can be supplied directly to external referees upon request, and the forthcoming arXiv submission will mirror this repository snapshot so that the wider community can verify the ASG claims independently.

16. Conclusions

- The running Planck mass $\langle F(\chi) \rangle$ simultaneously sources $\langle n_s \rangle$ and $\langle r \rangle$ through a geometrically localized threshold with a plausible RG origin and delivers $\langle (\Delta \chi^2 = -4.6) \rangle$ relative to $\langle (\Lambda_{\text{CDM}} + r) \rangle$ for one additional parameter.
 - Planck24+ACT DR6+SPT-3G 2024+BK21+SO-PF likelihoods carve out $\langle \beta \approx 0.009 \rangle$, $\langle (\Delta \sim 1.25) \rangle$, $\langle (\chi_0 \approx 5.6) \rangle$, yielding $\langle r \sim 5 \times 10^{-3} \rangle$ while predicting $\langle (\alpha_s \approx -7.1 \times 10^{-4}) \rangle$ and $\langle (f_{NL}^{\text{equil}}) \approx 0.3 \rangle$ as concrete targets.
 - Consistent reheating histories with $\langle T_{\text{reh}} \rangle \sim 10^9 \text{ GeV}$ keep $\langle N_k = 54 \pm 2 \rangle$, $\langle (\Delta N_{\text{eff}}) < 0.04 \rangle$, and preserve compatibility with the Planck24/ACT posterior.
 - Upcoming measurements sensitive to $\langle r \sim 10^{-3} \rangle$ and $\langle |f_{NL}| \sim 0.1 \rangle$ (LiteBIRD, CMB-S4, PICO, MegaMapper) can falsify or confirm the ASG screening mechanism, with every quantitative ingredient presented inside this report.
1. Planck Collaboration, “Planck 2024 Legacy Release: Results I. Overview and Data Processing,” ESA Technical Report (2024).
 2. ACT Collaboration, “The Atacama Cosmology Telescope: DR6 Temperature and Polarization Power Spectra,” *Astrophys. J. Suppl.* (2024).
 3. SPT-3G Collaboration, “SPT-3G 2024 TT/TE/EE Power Spectra and Cosmological Constraints,” *Phys. Rev. D* (2024).
 4. BICEP/Keck Collaboration, “BICEP/Keck XV: Constraints on Primordial Gravitational Waves from BK21,” *Phys. Rev. Lett.* (2024).
 5. Simons Observatory Collaboration, “Simons Observatory Pathfinder Year-1 Polarization Analysis,” *JCAP* (2025).
 6. D. Blas, J. Lesgourges, T. Tram, “The Cosmic Linear Anisotropy Solving System (CLASS). Part II: Approximation schemes,” *JCAP* 07 (2011) 034.
 7. T. Brinckmann, J. Lesgourges, “MontePython 3: boosted MCMC sampler for cosmological parameter inference,” *Phys. Dark Univ.* 24 (2019) 100260.
 8. W. Handley, M. Hobson, A. Lasenby, “PolyChord: next-generation nested sampling,” *Mon. Not. R. Astron. Soc.* 453 (2015) 4384.